観測的宇宙論速報 2010/05/24 Toshiya Namikawa

1. Mass Function Predictions Beyond ΛCDM

Bhattacharya, S., Heitmann, K., White, M., Lukic, Z., Wagner, G. and Habib, S.

arXiv : 1005.2239

2. Neutrino in Non-linear Structure Formation – The Effect on Halo Properties

Brandbyge, J., Hannestad, S., Troels, H. and Wong, Y. arXiv : 1004.4105

3. Evidence for the accelerated expansion of the Universe from weak lensing tomography with COSMOS

Schrabback, T. *et al* arXiv : 0911.0053

1 Mass Function Predictions Beyond ΛCDM

シミュレーションのパラメータ範囲

$$0.120 \le \omega_m \le 0.155,$$
$$0.0215 \le \omega_b \le 0.0235,$$
$$0.85 \le n_s \le 1.05,$$
$$-0.130 \le w \le -0.70,$$
$$0.61 \le \sigma_8 \le 0.90.$$

TABLE 2
SPECIFICATIONS OF THE SIMULATION RUNS

Box size	Name	n_p	m_p	$n_h^{\rm min}$	ϵ	Code	$z_{\rm in}$	$z_{\rm out}$	$N_{\rm runs}$	ICs
				ΛCDM						
1000 Mpc	C	1500^3	$1.1 \cdot 10^{10}\,M_\odot$	400	24 kpc	TreePM	100/75	0	2	ZA/2LPT
1736 Mpc	B	1200^3	$1.1 \cdot 10^{11}\,M_\odot$	400	51 kpc	TreePM	100	0, 1	6	2LPT
2778 Mpc	A	1024^3	$7.2 \cdot 10^{11}\,M_\odot$	400	97 kpc	TreePM	100	0, 1	10	2LPT
178 Mpc	GS	512^3	$1.5 \cdot 10^{9}\,M_\odot$	400	14 kpc	GADGET-2	211	0, 1, 2	10	ZA
1300 Mpc	G	1024^3	$7.4 \cdot 10^{10}\,M_\odot$	400	50 kpc	GADGET-2	211	0, 1, 2	2	ZA
				wCDM						
1300 Mpc	Coyote	1024^3	varies	400	50 kpc	GADGET-2	211	0, 1, 2	37	ZA

Note. — Box size, mass and force resolution for the different runs; the upper section of the table describes the ΛCDM simulation suite (model 0 in Table 1) while the lower section specifies the Coyote Universe runs (models 1 - 37 in Table 1). The total number of particles is denoted by n_p, the particle mass by m_p, $n_h^{\rm min}$ the number of particles in the smallest halo kept, ϵ the force resolution, and $N_{\rm runs}$ the number of realizations. For some simulations we used the Zel'dovich approximation (Zel'dovich 1970) (see also discussions in Lukić et al. 2007 and Heitmann et al. 2010) to generate the initial condtions and 2LPT (Bouchet et al. 1995, Crocce et al. 2006) for others.

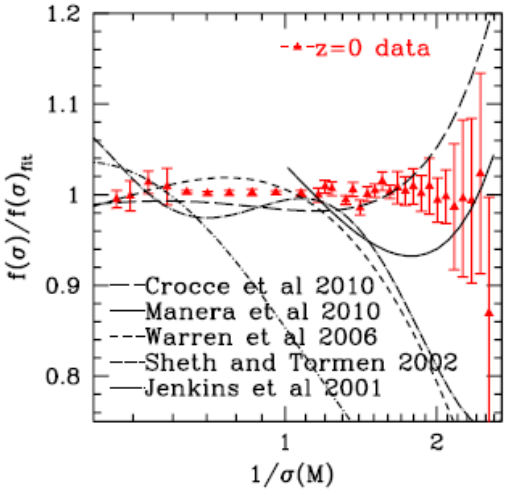

FIG. 4.— Ratio of various mass function fits derived in previous studies with respect to the results of this paper at $z = 0$. The binned numerical data are the points with error bars; the ratios are taken with respect to the analytic fit to the numerical data specified by Equation (12).

TABLE 4
MASS FUNCTION FITTING FORMULA DERIVED IN THIS STUDY, VALID OVER A MASS RANGE OF $(6 \times 10^{11} - 3 \times 10^{15})\,M_\odot$ AND OVER A REDSHIFT RANGE OF z=0-2.

$$f^{\rm mod}(\sigma, z) = \tilde{A}\sqrt{\frac{2\tilde{a}}{\pi}}\exp\left[-\frac{\tilde{a}\delta_c^2}{2\sigma^2}\right]\left[1+\left(\frac{\sigma^2}{\tilde{a}\delta_c^2}\right)^{\tilde{p}}\right]\left(\frac{\delta_c}{\sigma}\right)^{\tilde{q}}$$

Redshift Evolution

$$\tilde{A} = \frac{0.333}{(1+z)^{0.11}},\ \tilde{a} = \frac{0.788}{(1+z)^{0.01}},\ \tilde{p} = \frac{0.807}{(1+z)^{0.6}},\ \tilde{q} = \frac{1.795}{(1+z)^{0.6}}$$

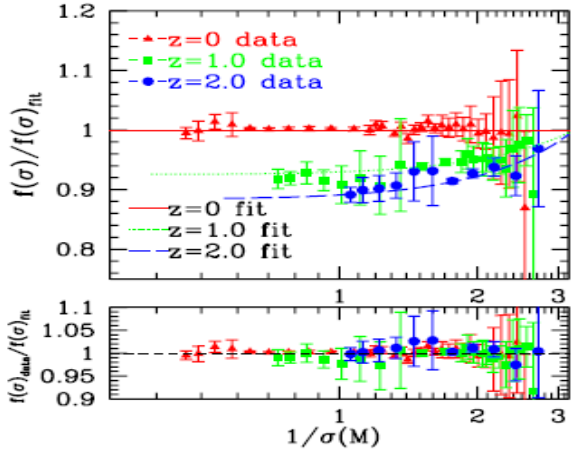

FIG. 5.— Ratio of the mass function data to the $z = 0$ fit of Equation (12) (reference flat red line). The $z = 1$ and $z = 2$ datasets demonstrate that redshift evolution is important and must be taken into account; the curves show the corresponding fits following the time-dependence as parameterized in Equations (14). The lower panel shows the ratio of the measured mass function at the three different redshifts to the corresponding analytic fits.

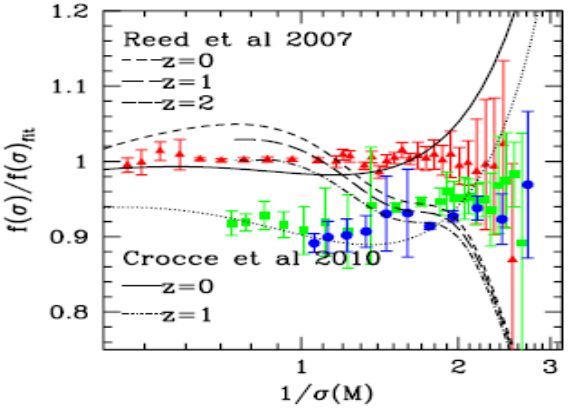

FIG. 6.— Redshift dependent mass function fits as introduced by Reed et al. (2007) and Crocce et al. (2010) compared with the numerical data of this work. Aside from disagreement in the overall shape, the results of Reed et al. (2007) underestimate the amount of evolution indicating that high redshift evolution of the mass function is slower compared to that at lower redshift. The agreement with Crocce et al. (2010) is better (at the 4-5% level), except for the runaway at high masses (see discussion in Section 4.1).

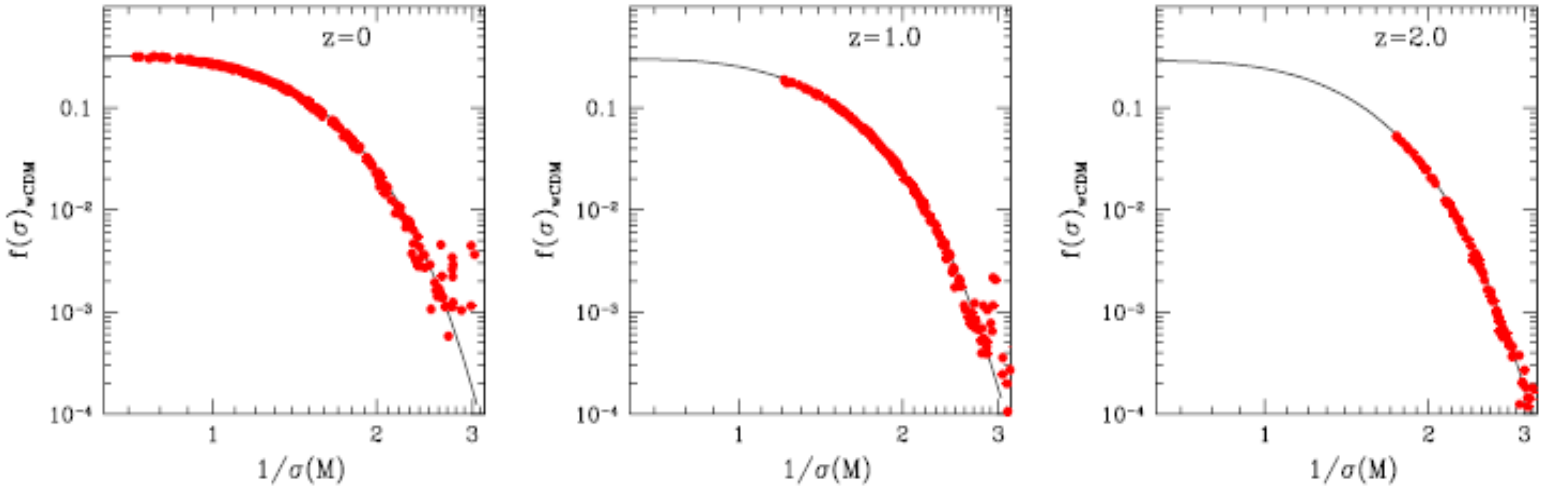

FIG. 13.— Approximate universality of the *w*CDM mass functions, all 37 models shown together.

2 Neutrino in Non-linear Structure Formation – The Effect on Halo Properties

	$N_{\rm CDM}$	$N_{\nu,\rm grid}$	$N_{\nu,\rm part}$	$q_{\rm cut}/T$	$f_{\rm flow}$	$R_{\rm BOX}$ $[h^{-1}{\rm Mpc}]$	$\sum m_\nu$ [eV]	Ω_ν [%]	Ω_m [%]
A_1	512^3	0	0	0	-	256	0	0	30
A_2	512^3	512^3	0	0	0	256	0.15	0.325	30
A_3	512^3	512^3	0	0	0	256	0.3	0.65	30
A_4	512^3	512^3	$6\cdot512^3$	6	4	256	0.6	1.3	30
A_5	512^3	512^3	$6\cdot512^3$	6	4	256	1.2	2.6	30
B_1	512^3	0	0	0	-	1024	0	0	30
B_2	512^3	512^3	0	0	0	1024	0.15	0.325	30
B_3	512^3	512^3	0	0	0	1024	0.3	0.65	30
B_3'	512^3	512^3	$6\cdot512^3$	6	4	1024	0.3	0.65	30
B_4	512^3	512^3	$6\cdot512^3$	6	4	1024	0.6	1.3	30
B_5	512^3	512^3	$6\cdot512^3$	6	4	1024	1.2	2.6	30
C_1	512^3	0	0	0	-	4096	0	0	30
C_2	512^3	512^3	0	0	0	4096	0.15	0.325	30
C_3	512^3	512^3	0	0	0	4096	0.3	0.65	30
C_4	512^3	512^3	$6\cdot512^3$	6	4	4096	0.6	1.3	30
C_5	512^3	512^3	$6\cdot512^3$	6	4	4096	1.2	2.6	30
D_1	512^3	0	0	0	-	256	0	0	28.7
D_2	512^3	0	0	0	-	1024	0	0	28.7
D_3	512^3	0	0	0	-	4096	0	0	28.7
E_1	512^3	0	0	0	-	256	0.6	1.3	30
E_2	512^3	0	0	0	-	1024	0.6	1.3	30
E_3	512^3	0	0	0	-	4096	0.6	1.3	30
E_4	512^3	0	0	0	-	256	0.6	1.3	30
E_5	512^3	0	0	0	-	1024	0.6	1.3	30
E_6	512^3	0	0	0	-	4096	0.6	1.3	30

Table 1. N-body simulation parameters: $N_{\rm CDM}$ and $N_{\nu,\rm part}$ are the number of CDM and neutrino N-body particles respectively, $N_{\nu,\rm grid}$ the size of the linear neutrino Fourier grid, $q_{\rm cut}/T$ the cut-off below which the neutrino component is converted to particles, and $f_{\rm flow}$ determines the redshift of this conversion. The simulation box size is represented by $R_{\rm BOX}$, $\sum m_\nu$ is the total neutrino mass roughly related to the neutrino density parameter, Ω_ν, by $\Omega_\nu = \sum m_\nu/(94\,h^2{\rm eV})$, with $\Omega_m = \Omega_c + \Omega_b + \Omega_\nu$. The exotic simulations E_{1-3} have no δ_ν in the N-body simulation, but the neutrinos are still included in the background evolution, while E_{4-6} have a CDM N-body particle mass corresponding to $\Omega_m = 0.3$ and the ICs are calculated from weighed CDM and baryon TFs from a cosmology with neutrinos included.

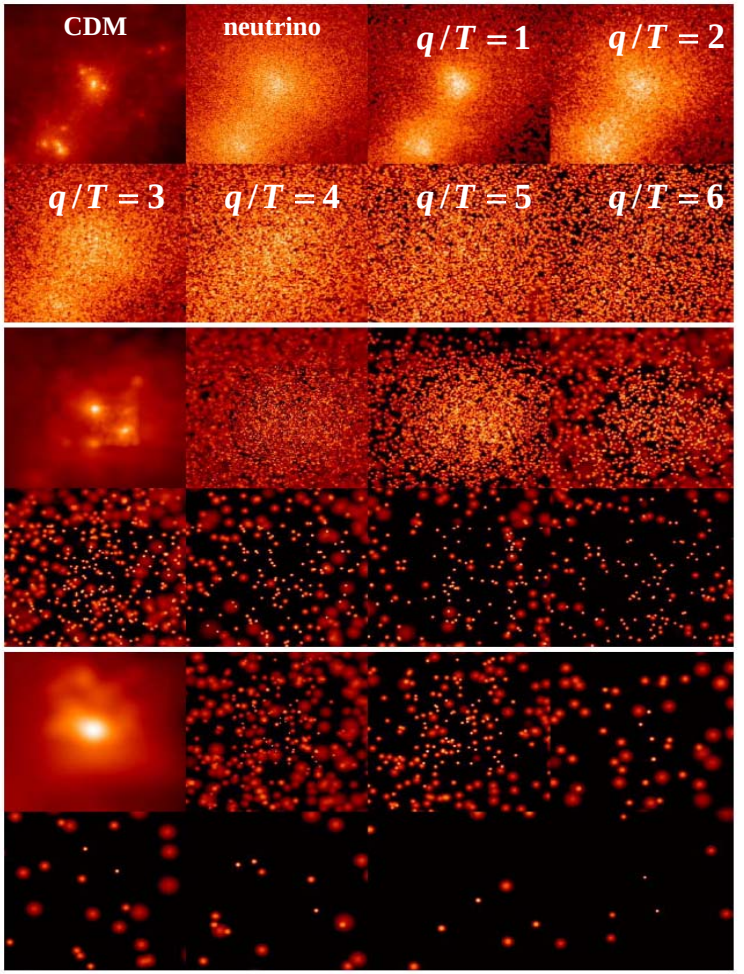

Figure 1. CDM and $\sum m_\nu = 1.2\,{\rm eV}$ neutrino distributions for halo masses $\simeq 5\cdot10^{14}{\rm M}_\odot$ (top), $\simeq 10^{14}{\rm M}_\odot$ (middle) and $\simeq 10^{13}{\rm M}_\odot$ (bottom), where the masses only correspond to the central halos in the upper two mosaics. Dimensions in each image are 5, 2 and 1 h^{-1} Mpc, respectively. In each mosaic the images correspond to CDM, total neutrino, and $q/T = 1$ to 6 from top-left to bottom-right. Individual neutrino N-body particles can be identified.

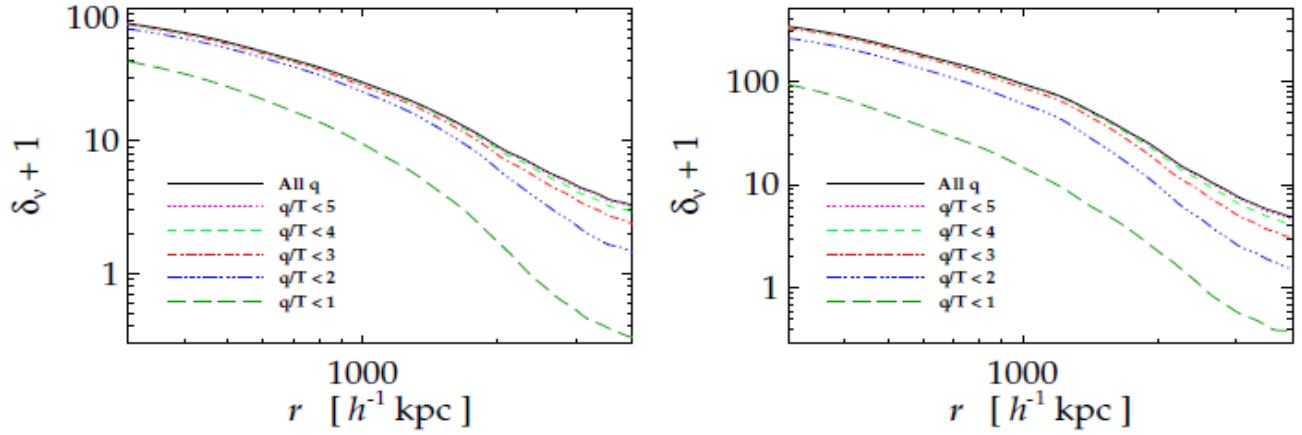

Figure 4. Cumulative neutrino halo density profiles as a function of momentum in a $10^{15}\mathrm{M}_\odot$ halo, for $\sum m_\nu = 0.6\,\mathrm{eV}$ (left) and $\sum m_\nu = 1.2\,\mathrm{eV}$ (right). The neutrino density with $q/T > 6$ has been added as a homogeneous term to all profiles.

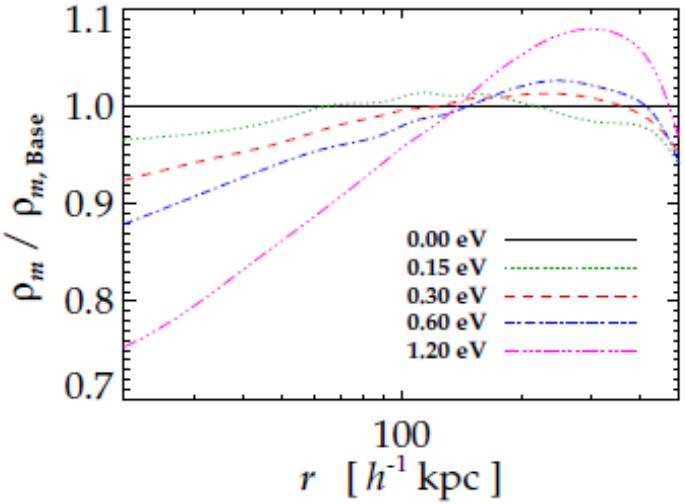

Figure 6. Change in the matter halo profiles relative to a base model without massive neutrinos for a halo mass of $10^{13}\,\mathrm{M}_\odot$.

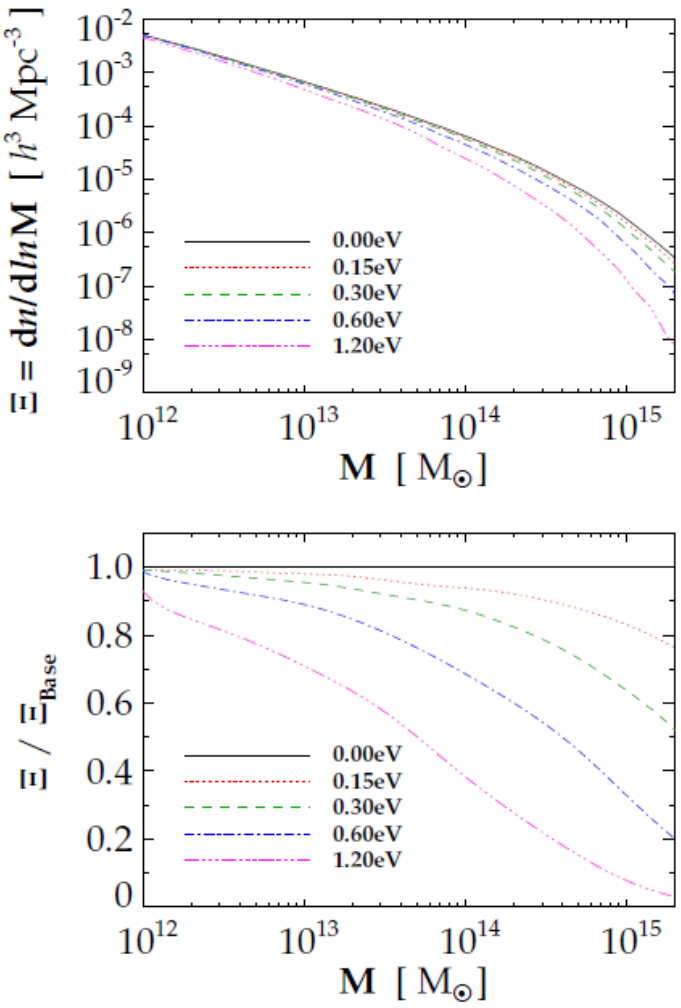

Figure 7. Absolute (top) and relative (middle) halo mass functions for 5 different neutrino cosmologies. The halo mass functions have been splined and smoothed together to obtain sufficient accuracy in the halo mass range 10^{12} to 10^{15} $M_\odot$. Bottom: Relative change in our halo mass function for different (exotic) cosmologies.

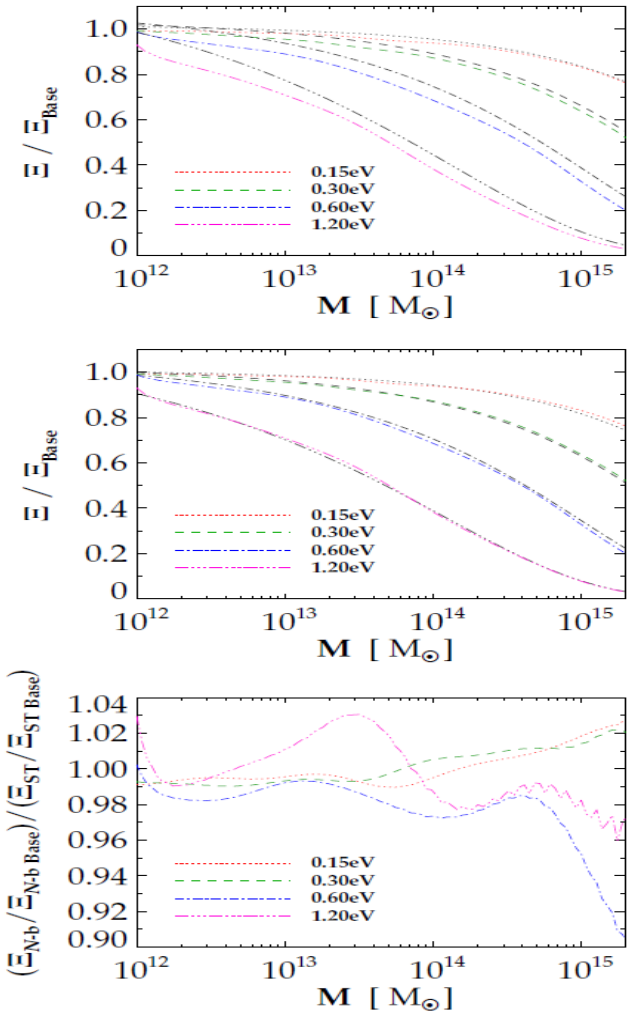

Figure 8. Relative halo mass functions for different neutrino cosmologies compared with the predictions from the Sheth-Tormen formulae (black lines). Top: With $\Omega_m = \Omega_c + \Omega_b + \Omega_\nu$ in the ST formulae. Middle: With $\Omega_c + \Omega_b$ used instead of Ω_m in the ST formulae. Bottom: Differences between the N-body and the ST predictions.

3 Evidence for the accelerated expansion of the Universe from weak lensing tomography with COSMOS

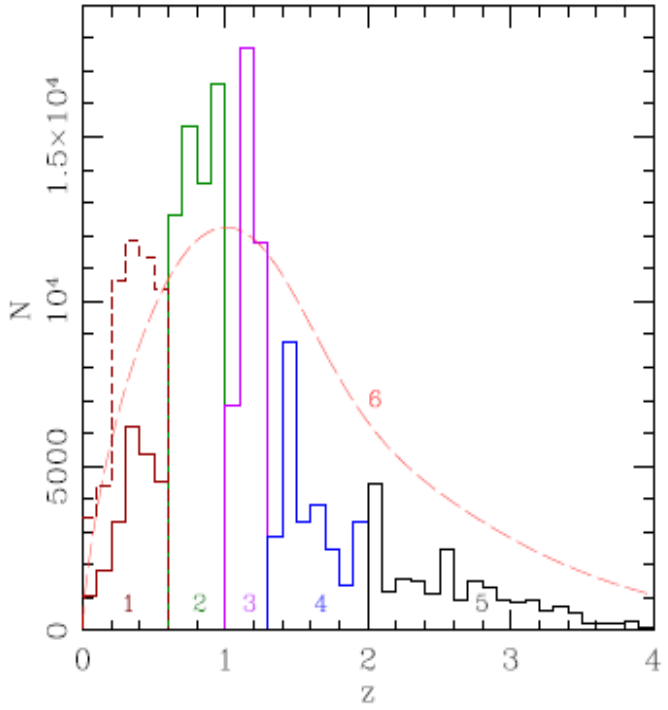

Fig. 6. Redshift distributions for our tomography analysis. The solid-line histogram shows the individual COSMOS-30 redshifts used for bins 1 to 5, while the difference between the dashed and solid histograms indicates the $24 < i^+ < 25$ galaxies with $z_{\rm phot} < 0.6$, which are excluded in our analysis due to potential contamination with high-redshift galaxies. The long-dashed curve corresponds to the estimated redshift distribution for $i_{814} < 26.7$ shear galaxies without individual COSMOS-30 photo-z, which we use as bin 6.

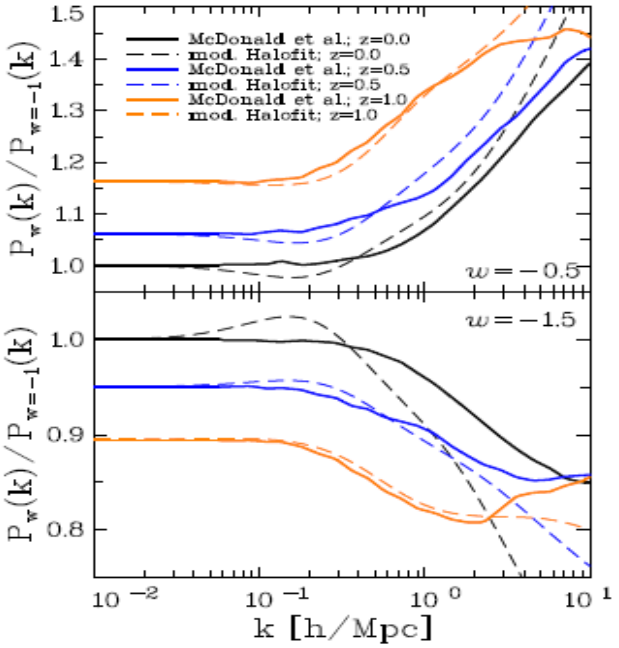

Fig. 10. Comparison of the fit formulae for the non-linear growth of structure in wCDM cosmologies. Shown is the three-dimensional matter power spectrum, normalized by the corresponding ΛCDM power spectrum, as a function of the wave vector k. In the upper panel we consider a wCDM cosmology with $w = -0.5$, in the lower panel one with $w = -1.5$. Solid curves show the fit to the simulations by McDonald et al. (2006), while the dashed lines have been obtained by interpolating the Smith et al. (2003) fitting formulae between the cases of an OCDM and a ΛCDM cosmology as outlined in Sect. 6.2. Each fit formula has been computed at redshifts $z = 0$ (black), $z = 0.5$ (blue), and $z = 1$ (orange). While deviations are substantial at $z = 0$, the lensing analysis of the deep COSMOS data is mostly sensitive to structures at $z \gtrsim 0.4$, where deviations are reasonably small. Note that the remaining cosmological parameters have been set to their default WMAP5-like values, except for $\sigma_8 = 0.9$.

Table 2. Constraints on $\sigma_8\,(\Omega_m/0.3)^\alpha$, Ω_m, Ω_{DE}, and w from the COSMOS data for different cosmological models and analysis schemes, using our default priors. We quote the marginalized mean and 68.3% confidence limits (16th and 84th percentiles) assuming non-linear power spectrum corrections according to Smith et al. (2003) and the description given in Sect. 6.2. Our analysis of the Millennium Simulation (Sect. 6.4) suggests that the σ_8-estimates should be reduced by a factor $\times 0.95$ due to biased model predictions for the non-linear power spectrum and reduced shear corrections. The power-law slopes α have typical fit uncertainties of $\sigma_\alpha \simeq 0.02$.

Cosmology	Analysis	α	$\sigma_8\,(\Omega_m/0.3)^\alpha$	Ω_m	Ω_{DE}	w
Flat ΛCDM	3D	0.51	0.79 ± 0.09	$0.32^{+0.34}_{-0.11}$	$0.68^{+0.11}_{-0.34}$	-1
Flat ΛCDM	2D	0.62	0.68 ± 0.11	$0.30^{+0.44}_{-0.15}$	$0.70^{+0.15}_{-0.44}$	-1
General ΛCDM	3D	0.77	0.74 ± 0.12	$0.43^{+0.40}_{-0.19}$	$0.97^{+0.39}_{-0.60}$	-1
Flat wCDM	3D	0.47	0.79 ± 0.09	$0.30^{+0.39}_{-0.11}$	$0.70^{+0.11}_{-0.39}$	$-1.23^{+0.79}_{-0.50}$

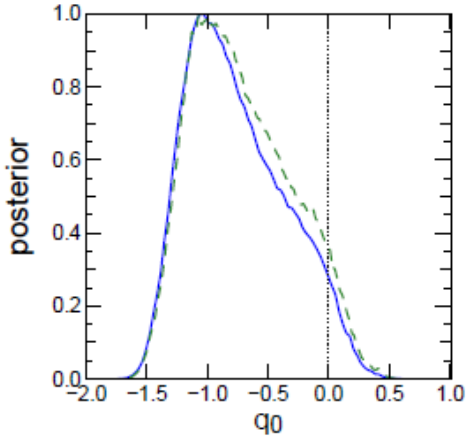

Fig. 13. Posterior PDF for the deceleration parameter q_0 as computed from our constraints on Ω_m and Ω_Λ for a general (non-flat) ΛCDM cosmology, using our default priors (solid curve), and using weaker priors from the HST Key Project and Big-Bang nucleosynthesis (dashed curve). The line at $q_0 = 0$ separates accelerating ($q_0 < 0$) and decelerating ($q_0 > 0$) cosmologies. We find $q_0 < 0$ at 96.0% confidence using our default priors, or 94.3% confidence for the weaker priors.